

Predictions of solute transport in a compound channel using turbulence models

Prédiction du transport de substance dissoute dans un canal composé en utilisant des modèles de turbulence

SHIONO, K. and SCOTT, C.F., *Department of Civil and Building Engineering, Loughborough University, UK*

KEARNEY, D., *Binnie Black & Veatch Ltd, 38 City Road, Chester, CH1 3AE, UK*

ABSTRACT

Prediction of solute distributions in an asymmetric compound channel is carried out using two turbulence models. Results of the numerical models are compared with turbulence data recently obtained using laser Doppler anemometer (LDA) and laser induced fluorescence (LIF) in a small laboratory flume. The predicted distributions of solute and Reynolds flux using a $k-\varepsilon$ model and an algebraic stress model for various injection points near the water surface are used to identify different mixing mechanisms. A skewed distribution of solute on the floodplain observed in the experimental data is well predicted by the algebraic stress model but not by the $k-\varepsilon$ model. The cause of the skewed distribution is examined through the variations of secondary flow and eddy diffusivity. The predicted eddy viscosity and diffusivity and the turbulent Schmidt number are discussed with the experimental data. As a result, solute concentration distribution can be well predicted by adjusting the turbulent Schmidt number even if the eddy viscosity was not correctly calculated by any particular model. An effect of secondary flow on peak concentration in the shear layer along the channel is also demonstrated.

RÉSUMÉ

La prédiction des distributions de substances dissoutes dans un canal composé asymétrique est effectuée en utilisant deux modèles de turbulence. Les résultats des modèles numériques sont comparés aux données de turbulence obtenues récemment par anémométrie laser Doppler (LDA) et laser à fluorescence induite (LIF) dans un petit canal expérimental. Les distributions prédites pour la substance dissoute et les flux de Reynolds, par un modèle $k-\varepsilon$ et un modèle de contrainte algébrique, pour divers points d'injection près de la surface, sont utilisées pour identifier différents mécanismes de mélange. Une répartition oblique de la solution sur le lit majeur, observée expérimentalement, est bien prédite par le modèle algébrique mais pas par le modèle $k-\varepsilon$. La cause de cette répartition oblique est recherchée dans les variations de l'écoulement secondaire et de la diffusivité turbulente. La viscosité et la diffusivité turbulentes calculées ainsi que le nombre de Schmidt turbulent sont confrontés aux données expérimentales. Il en résulte que la concentration de la solution peut être convenablement prédite en ajustant le nombre de Schmidt turbulent, même si la viscosité turbulente n'est correctement calculée par aucun modèle particulier. On démontre aussi un effet de l'écoulement secondaire sur le pic de concentration dans la couche de cisaillement le long du canal.

Keywords: Numerical model; solute transport; compound channel; mixing coefficients; Reynolds fluxes.

1 Introduction

Most natural rivers have a flood plain that extends laterally away from the main channel at a gentle gradient or a series of terraces. River channels such as this are typically called compound channels. When flooding occurs, the fast flow in the main channel is retarded by the slower moving flow on the flood plain, thereby causing a large lateral exchange of momentum. The shear layer generated by the difference in velocity affects the turbulence structure and vortices develop in the longitudinal axis. These effects have been observed by Shiono and Knight (1991), Tominaga and Nezu (1991) and Naot *et al.* (1993). They have found that secondary currents have significant influence on momentum transfer and boundary shear stress. Therefore

transport processes of pollutants could be different from those in wide rivers studied in the past.

Wood and Liang (1989) measured tracer concentration in a series of experiments in a compound channel and also developed a two-dimensional semi-analytical model to predict solute transport. Djordjevic (1993) developed a two-dimensional numerical model to predict the unsteady solute transport rates in a compound channel and verified his model experimentally. A three-dimensional eigenfunction solution for solute dispersion in wide rectangular channels was presented by Nokes and Wood (1988) and extended by Nokes and Hughes (1994) to include compound channel flows. Prinos (1992) developed a three-dimensional model in conjunction with the linear $k-\varepsilon$ model to study solute transport rates in compound channel flow. None of these methods

take into account the effect of secondary flow on pollutant transport as these models do not produce secondary flow. Lin and Shiono (1995) investigated solute transport in a compound channel using the linear and non-linear k - ε models and found significant difference in solute distributions with and without secondary flow. They also suggest that it may be inaccurate to assume a uniform Schmidt number for all points in the channel and for both vertical and lateral diffusion. This hypothesis was taken a step further by Simoes and Wang (1997) who used an an-isotropic arrangement of Schmidt number in a compound channel and obtained reasonable results. They concluded, however that they would have obtained better results if their model was able to account for secondary flow.

To date, there is limited data available for turbulence and secondary flow together with solute concentration and Reynolds fluxes to validate numerical turbulence models for solute transport. Shiono and Feng (2003) recently measured turbulent fluctuations of velocity and solute simultaneously using combined laser Doppler anemometer and laser induced fluorescence. This provided a new set of turbulence data including three components of velocity, turbulence intensities and Reynolds stresses together with solute concentration and Reynolds fluxes. This paper presents an investigation of secondary flow effect on solute transport processes in a compound channel using the new experimental data and two numerical turbulent models. One model produces secondary flow while the other model does not.

2 Mean flow equations

The governing equations of continuity and momentum can be written for steady and uniform flow in a compound channel as follows. The continuity equation:

$$\frac{\partial U}{\partial x} + \frac{\partial V}{\partial y} + \frac{\partial W}{\partial z} = 0 \quad (1)$$

where x is the stream-wise co-ordinate, y is the transverse co-ordinate, z is the vertical co-ordinate, U is the mean stream-wise velocity, V is the mean lateral velocity, W is the mean vertical velocity. The momentum equations, ignoring the rate of change of Reynolds stresses in the x -direction, $-\partial u^2/\partial x$, $-\partial \bar{u}v/\partial x$ and $-\partial \bar{u}w/\partial x$ since the flow is uniform, are given by Eqs. (2)–(4):

$$U \frac{\partial U}{\partial x} + V \frac{\partial U}{\partial y} + W \frac{\partial U}{\partial z} = \left(-g \frac{\partial H}{\partial x} + g \sin \theta \right) - \frac{\partial}{\partial y} \bar{u}v - \frac{\partial}{\partial z} \bar{u}w \quad (2)$$

$$U \frac{\partial V}{\partial x} + V \frac{\partial V}{\partial y} + W \frac{\partial V}{\partial z} = -\frac{1}{\rho} \frac{\partial P}{\partial y} - \frac{\partial}{\partial y} \bar{v}^2 - \frac{\partial}{\partial z} \bar{v}w \quad (3)$$

$$U \frac{\partial W}{\partial x} + V \frac{\partial W}{\partial y} + W \frac{\partial W}{\partial z} = -\frac{1}{\rho} \frac{\partial P}{\partial z} - \frac{\partial}{\partial y} \bar{v}w - \frac{\partial}{\partial z} \bar{w}^2 \quad (4)$$

where g is acceleration due to gravity, ρ the fluid density, H the local channel depth, $-\bar{u}w$, $-\bar{u}v$, and $-\bar{v}w$ the Reynolds stresses, u , v and w are the fluctuations against the mean values, U , V and W , respectively.

3 Turbulent models

3.1 Linear k - ε model

The standard k - ε turbulence model as classified as a two-equation model since it uses two transport equation to characterize the turbulence. The two transport equations are given by Rodi (1980) as follows:

Turbulent kinetic energy equation:

$$U \frac{\partial k}{\partial x} + W \frac{\partial k}{\partial z} + V \frac{\partial k}{\partial y} = \frac{\partial}{\partial z} \left(\frac{\nu_t}{\sigma_k} \frac{\partial k}{\partial z} \right) + \frac{\partial}{\partial y} \left(\frac{\nu_t}{\sigma_k} \frac{\partial k}{\partial y} \right) + \pi - \varepsilon \quad (5)$$

Turbulent kinetic energy dissipation rate equation:

$$U \frac{\partial \varepsilon}{\partial x} + W \frac{\partial \varepsilon}{\partial z} + V \frac{\partial \varepsilon}{\partial y} = \frac{\partial}{\partial z} \left(\frac{\nu_t}{\sigma_\varepsilon} \frac{\partial \varepsilon}{\partial z} \right) + \frac{\partial}{\partial y} \left(\frac{\nu_t}{\sigma_\varepsilon} \frac{\partial \varepsilon}{\partial y} \right) + C_{\varepsilon 1} \frac{\varepsilon}{k} \pi - C_{\varepsilon 2} \frac{\varepsilon^2}{k} \quad (6)$$

where π = production of energy by the mean velocity gradients given as

$$\pi = \nu_t \left(\frac{\partial U}{\partial z} \right)^2 + \nu_t \left(\frac{\partial U}{\partial y} \right)^2 \quad (7)$$

The coefficients in Eq. (6) are given by Naot and Rodi (1982) as $C_{\varepsilon 1} = 1.44$; $C_{\varepsilon 2} = 1.92$; $\sigma_k = 1.225$; $\sigma_\varepsilon = 1.225$. The eddy viscosity is defined as:

$$\nu_t = \frac{C_\mu k^2}{\varepsilon} \quad (8)$$

where $C_\mu = 0.09$.

Reynolds stresses are expressed in the tensor form

$$-\bar{u}_i u_j = \nu_t \left(\frac{\partial U_i}{\partial x_j} + \frac{\partial U_j}{\partial x_i} \right) - \frac{2}{3} k \sigma_{i,j} \quad (9)$$

where $i, j = 1, 2, 3$ and $\delta_{i,j} = 1$ for $i = j$ and $\delta_{i,j} = 0$ for $i \neq j$.

3.2 Secondary flow models

Models used that produce secondary flow in compound channels are as follows. Launder and Ying (1973) and Naot and Rodi (1982) have developed the algebraic Reynolds stress models for a duct and a rectangular open channel which were modified for compound channel flow by Kawahara and Tamai (1988) and Naot *et al.* (1993) respectively. A non-linear k - ε model developed by Speziale (1987) has been modified for open compound channel flow by Shiono and Lin (1992) and Pezzinga (1994). The full Reynolds-stress transport model has been developed by Cokljak and Younis (1995) to simulate flows in open compound channels and a large eddy simulation has also been applied to compound channels (Thomas and Williams, 1995). There are a number of other numerical methods for generating secondary flow in an open channel. Kearney (2000) used three models (Launder and Ying, Naot and Rodi and Speziale models) to study solute transport in a compound channel and reported that the LY gives slightly better prediction than the other models and the LKE model gives the worst prediction. The LY model is relatively easy to specify the normal Reynolds stresses and the cross Reynolds stresses and therefore was chosen in this paper.

3.2.1 Launder and Ying Model (LY)

$$\overline{v^2} = -C'v_t \frac{k}{\varepsilon} \left(\frac{\partial U}{\partial y} \right)^2 + C'_k k \quad (10)$$

$$\overline{w^2} = -C'v_t \frac{k}{\varepsilon} \left(\frac{\partial U}{\partial z} \right)^2 + C'_k k \quad (11)$$

$$\overline{vw} = \overline{wv} = -C'v_t \frac{k}{\varepsilon} \left(\frac{\partial U}{\partial y} \right) \left(\frac{\partial U}{\partial z} \right) \quad (12)$$

The values for the empirical constants are $C'_k = 0.522$ and $C' = 0.037$. The C' value controls the secondary flow magnitude.

4 Solute transport model

Assuming Fick's law to be valid and that the scale of random turbulent motion is very much greater than that of the molecular motion, the steady, three-dimensional solute transport equation of a passive contaminant can be written as:

$$U \frac{\partial C}{\partial x} + V \frac{\partial C}{\partial y} + W \frac{\partial C}{\partial z} = \frac{\partial}{\partial y} \left(D_y \frac{\partial C}{\partial y} \right) + \frac{\partial}{\partial z} \left(D_z \frac{\partial C}{\partial z} \right) \quad (13)$$

where C is the solute concentration, D_y and D_z are eddy diffusivity in the lateral and vertical directions, respectively. Note that the turbulent diffusion term in the stream-wise direction is ignored in the hydrodynamic model.

5 Boundary and initial conditions

There are three types of boundary condition in open channel flow.

- Plane of symmetry: the velocity component normal to the symmetric plane is zero, while the gradient normal to the plane is taken as zero for all other quantities.
- Solid wall: the wall function is adopted such that a resultant stream-wise velocity, U , is expressed by a local friction velocity at a first grid point to the wall of the computational domain.
- Free surface: a plane of symmetry where the conditions are applied for all variables except for the rate of turbulent energy dissipation. The expression for the dissipation rate given by Noat and Rodi (1982) at a first grid point the surface was adopted.
- The boundary condition to be imposed for solute transport is that no material is lost through the boundaries of the flow.

6 Numerical procedure

The SIMPLER method of Patanker and Spalding (1972) has been adopted to solve the models, which were assumed to be parabolic in the stream-wise direction but elliptic in the cross-stream planes. The solutions were obtained by marching the 2-D cross-section along the stream-wise direction until the flow became a fully developed turbulent flow over the distance, $x_l/H = 500$, where x_l is the longitudinal distance and H is the water depth in the

main channel. A staggered grid mesh was used, in which the secondary velocity components were placed at the sides the computational mesh, while all the other variables were placed at the centre of the mesh. The mesh sizes were set uniformly to 5 mm except near the solid wall boundaries where the mesh sizes were adjusted by the application of the wall function. For every step in the stream-wise direction, the velocity components and pressure were computed first, using the momentum and continuity Eqs. (1)–(4), then the turbulent kinetic energy and dissipation rate were computed using Eqs. (5) and (6), finally the Reynolds stresses were estimated using Eqs. (10)–(12). For the solute transport rate computation, the flow field and the turbulent quantities associated with the diffusion equation were assumed to be unchanged along the stream-wise direction after the flow was fully developed. Therefore the advection-diffusion Eq. (13) was solved using the fully developed velocity components and turbulence quantities obtained from the hydrodynamic model.

7 Experimental data

The flow and solute measurements in a compound channel were carried out by Shiono and Feng (2003). Three components of turbulent velocity were measured using a Laser Doppler Anemometer and the tracer concentrations were also simultaneously measured using a Laser Induced Fluorescence. The tracer used was a fluorescence dye (Rhodamine 6G), injected at a constant rate from a reservoir and via a 2 mm diameter nozzle.

Tests were carried out with two different water depths: the first with a depth of 100 mm, and the second shallow case with a depth of 75 mm. The compound channel geometry and dimensions are shown in Table 1 and Figure 1. The two discharges were $Q = 46.1$ l/s for the deep channel, and $Q = 22.6$ l/s for the shallow channel, both with a bed slope $S_0 = 1/2000$.

The tracer was injected in three positions in the deep channel, here after referred to as C1, C2 and C3, (see detail injection locations listed on Table 2). In the shallow channel, only one injection point was used, referred to as S1 in Table 2. The measurements were taken 1 m downstream of the injection nozzle and the dye injection flow rate was 54 ml/min with an initial concentration 2500 ppb for the deep water depth and 33 ml/min for the shallow water depth. All the measured data were corrected by applying mass conservation.

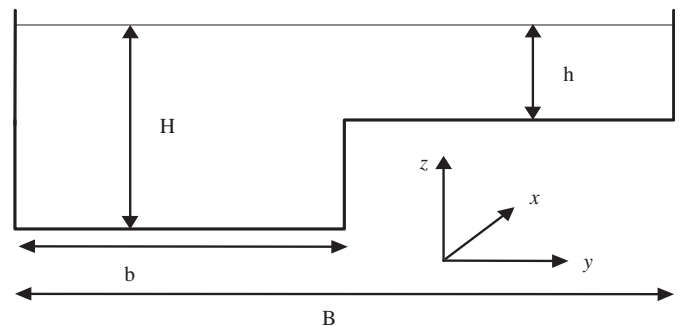


Figure 1 Compound channel.

Table 1 Flow characteristic parameters with channel dimensions.

Test case	Main channel depth H (m)	Flood plain depth h (m)	Main channel width b (m)	Flood plain width (m)	Bed slope S_0	Mean velocity U (m/s)	Bed friction velocity U^* (m/s)	Reynolds Number $Re (\times 10^3)$	Froude Number Fr
S1	0.075	0.02	0.1	0.1	0.0005	0.201	0.012	15.1	0.235
C1, 2, 3	0.11	0.055	0.1	0.1	0.0005	0.237	0.014	26.1	0.228

Table 2 Dye injection locations and measurement locations.

Test case	Dye injection location			Injection concentration (ppb)	Injection flow rate (ml/min)	Measurement locations (m)
	x (m)	y (m)	z (m)			
S1	13	0.1	0.073	2500	33	14
C1	13	0.05	0.108	2500	54	14
C2	13	0.1	0.108	2500	54	14
C3	13	0.15	0.108	2500	54	14

8 Justification of hydraulic models

8.1 Velocity

Figure 2a shows the measured isovels for stream-wise velocity, normalized by friction velocity, $U^* = \sqrt{gRS_0}$ where g is acceleration due to gravity, R is the hydraulic radius, and S_0 is the bed

slope. The bulging of the isovels towards the main channel away from the edge of the flood plain is characteristic of flows where secondary currents are present. The velocity maxima occur at mid-depth in the main channel and on the flood plain.

The stream-wise velocity predicted by the linear k- ϵ (LKE) model is shown in Figure 2b. This model does not produce the secondary flow, and accordingly its influence is not reflected in

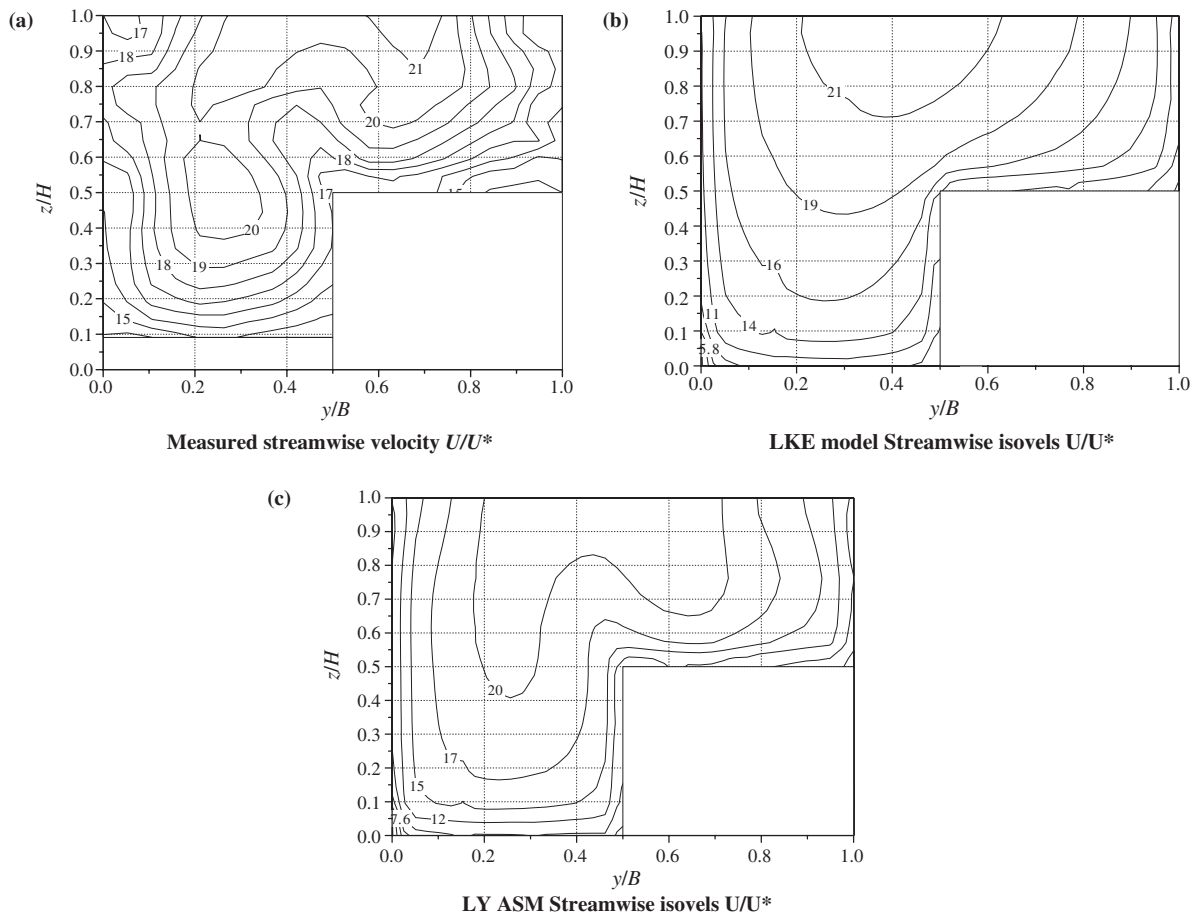


Figure 2 Measured and predicted velocity distributions.

the stream-wise velocity contours. There is no bulge in the isovels at the channel junction and the maximum velocity occurs at the surface. The velocity predicted by the LY model is plotted in Figure 2c. The model produces secondary flow and flow characteristics are evident in the stream-wise velocity distribution. The isoline of the maximum velocity of 20 bulges to approximately $0.8H$ near the channel step, but then drops to $0.4H$ in the centre of the main channel. The model predicts the characteristic of the compound channel flow well, and the result also is in good agreement with the experimental data nevertheless the angle of the bulging direction is steeper than the measured one.

Detailed vertical profiles of velocity at three locations in the shear layer for the LKE and LY model results and experimental data were presented here for validation of the numerical models. At $y = 75$ mm, it can be seen from Figure 3 that the results of the $k-\epsilon$ model are overestimated but that the results of the LY model agree well. The LY model also shows good agreement at the other two locations. The LKE model predicts less accurately in the shear layer region owing to its inability to predict the

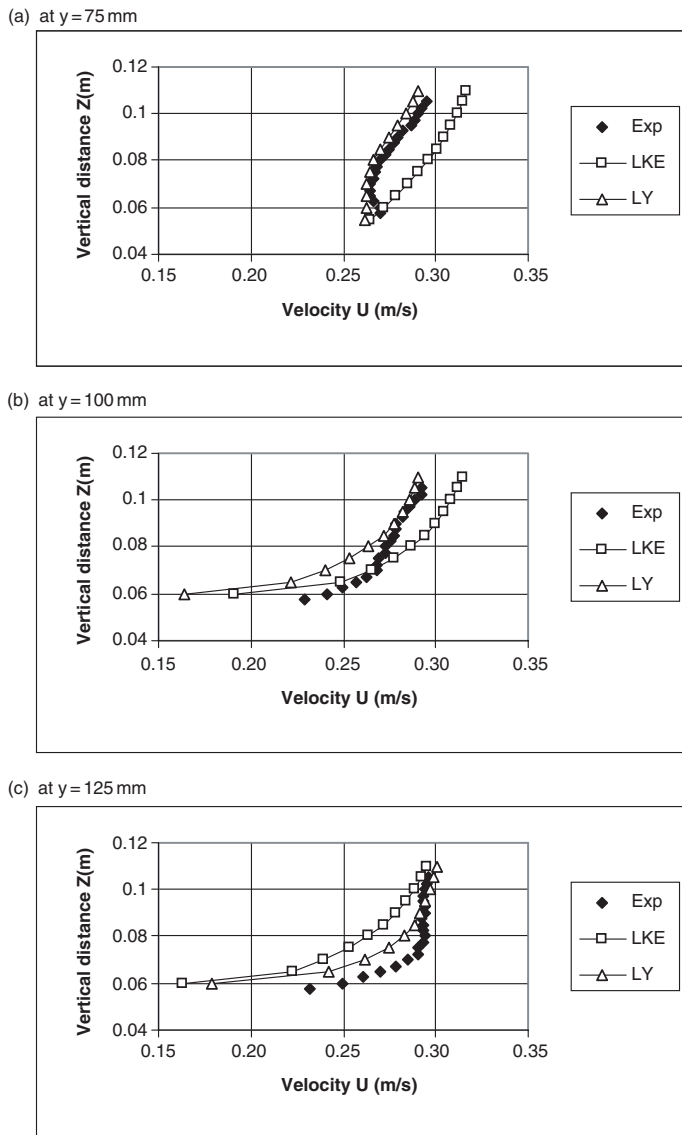


Figure 3 Velocity distributions of experimental data and model results for 100 mm injection point.

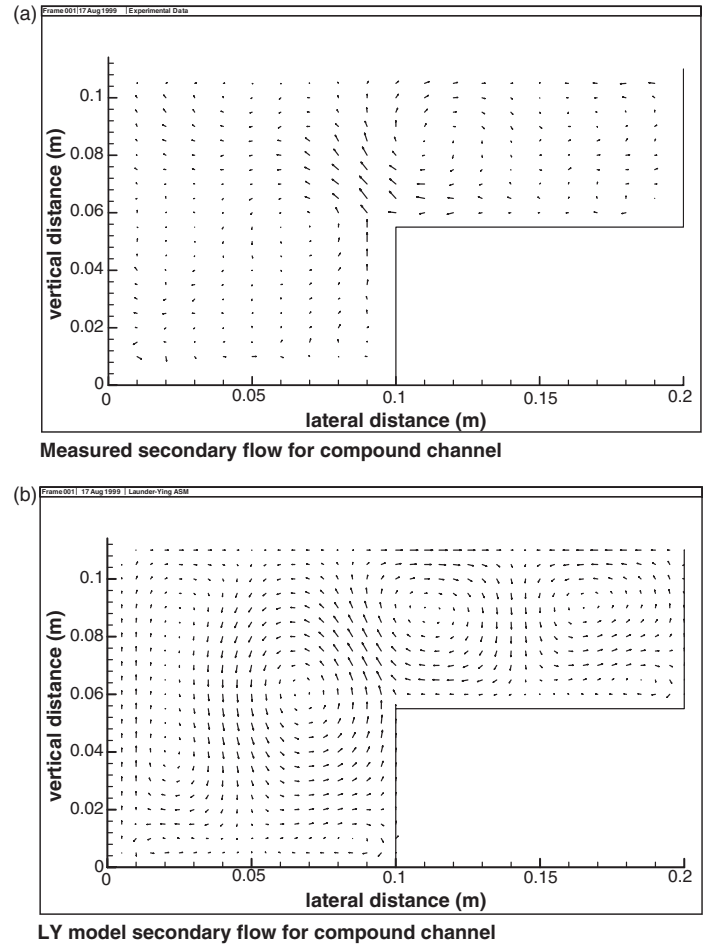


Figure 4 Measured and predicted secondary currents.

secondary flow. The secondary flow is therefore very important if the velocity is to be accurately predicted in the shear layer region.

8.2 Secondary flow

The measured secondary currents together with the secondary currents predicted by the LY model are shown in Figures 4a and b. It can be seen from the figures that there are twin vortices in the shear layer region and two more secondary flow cells on the floodplain, which is one of the compound channel flow characteristics. The LY model predicts well the twin vortices in the shear layer region and two more secondary flow cells on the floodplain. The magnitude of secondary currents corresponds closely with the experimental data. The inclination angle of two vortices from the edge of the main/floodplain junction is slightly steep as was also reported by Nezu (1996).

9 Solute prediction results

9.1 Lateral distribution of concentration in deep flooded water

A prediction of lateral distribution of solute concentration for deep flooded water in the $y = 50, 100$ and 150 mm injection cases (C1, C2 and C3) was carried out assuming the eddy diffusivity equal to the eddy viscosity (i.e. turbulent Schmidt number = 1.0).

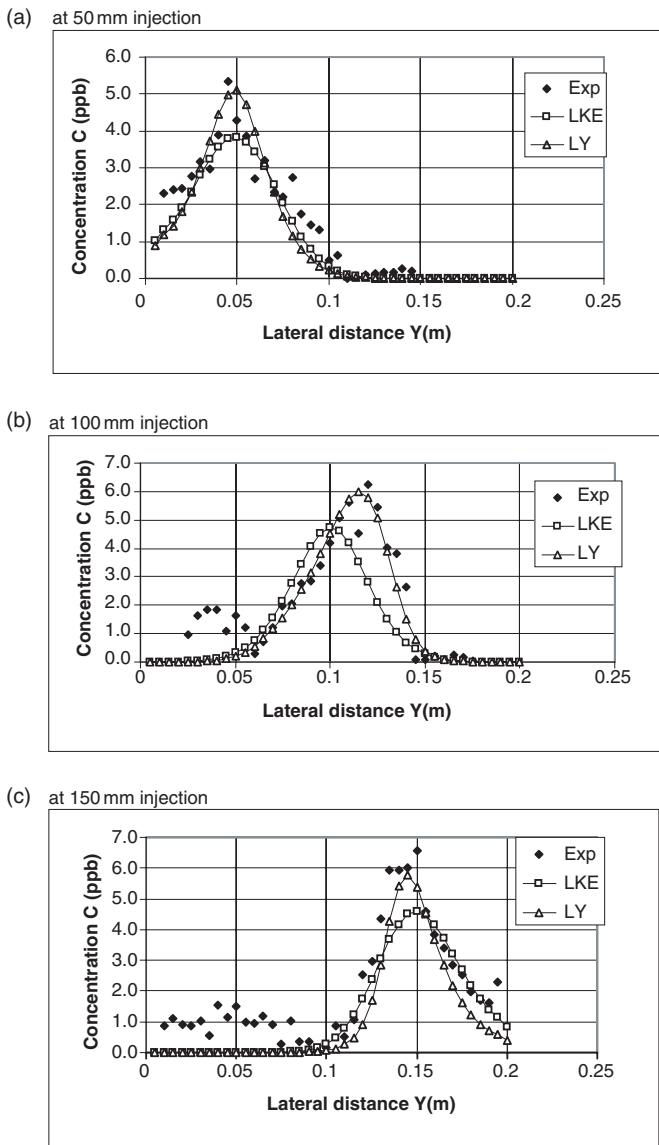


Figure 5 Mean concentration distributors near water surface for experimental data and models results.

For C1 dye concentration distributions are shown in Figure 5a. The experimental data shows a curve that peaks at approximately 5.3 ppb and the LY model slightly predicts lower peak, but considerably lower for the linear $k-\epsilon$ model (LKE), and also the spread of dye for both models is less than in the experimental data. The LKE model produces more or less a normal distribution, as expected as the result of no secondary flow. However the distribution is a little skewed, which could be caused by the variation of the eddy diffusivity in the lateral direction. The models predict lower concentration in most of regions implying that the mixing is being under predicted. Furthermore the experimental data curve is flatter than the numerically predicted curves, which suggests that the models are under-predicting the spreading of dye.

The distributions of the concentration for C2 as shown in Figure 5b are considerably skewed to the right. The LY model closely matches the experimental data in peak magnitude and peak position. The LKE model predicts again the lower peak concentration. For the C3 case, as can be seen in Figure 5c, the measured concentration peaks at 6.6 ppb, at a lateral distance

$y = 150$ mm, which is in line with the injection point. Again the LY model predicts a lower peak concentration of just under 6.0 ppb, and the LKE model predicts a further lower peak concentration of 4.0 ppb. The concentration gradients $\partial C/\partial y$ are well predicted by the LY model on the left side of the concentration peak, but not on the right side. However the LKE model predicts the gradient on the right side better.

9.2 Reynolds fluxes

For C1, the lateral Reynolds fluxes, shown in Figure 6a are well predicted on the left side of the zero flux by the LY model, but not by the LKE model, and both models under-predict the peak on the right side.

For C2, the experimental flux shown in Figure 6b is higher than the predicted fluxes, in both the positive and negative peaks. Both models under-predict the flux peaks. The LY model predicts

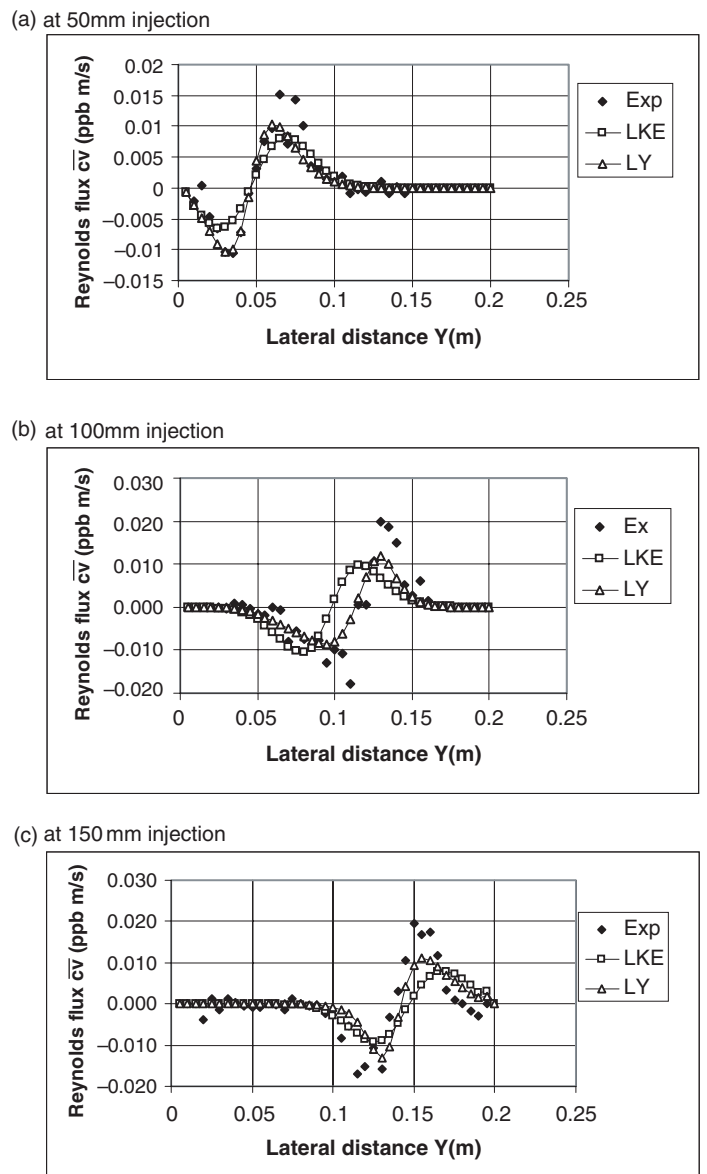


Figure 6 Reynolds flux, $\bar{c}v$, distributors of for experimental data and model results near water surface and 1 m downstream from injection point.

the locations of peak flux that coincide with the experimental flux peak locations but the LKE model does not.

For C3, both models again under-predict the flux peaks, and over-predict the flux in the region $y > 0.17$ m, but predict the magnitude of flux in the region $0.1 \text{ m} < y < 0.15$ m better than on the right side of the zero flux. The LKE model flux curve is shifted much further to the right, compared with the experimental data and the LY model prediction.

In summary, both models do not predict the Reynolds flux very well. However LY is moderately better prediction than LKE.

9.3 Vertical distributions

The experimental results together with the LKE and LY model predictions at $y = 75$, 100 and 125 mm in the shear layer region for C2 are shown in Figure 7. The LKE model under predicts the measured concentration at $y = 75$ mm, predicts well at $y = 100$ mm and over-predicts at $y = 125$ mm while the LY model gives a good prediction. Looking at the gradient of concentration, both models predict milder in the upper layer ($z > 95$ mm) than that of the experimental data and steeper in the lower layer, implying that the models over predict the mixing.

The distributions of the Reynolds flux, \overline{cw} , are shown in Figure 8 together with the predictions. Both models over-predict the measured flux and the LY model again gives better prediction than the LKE model.

9.4 Shallow flooded water

In S1, the water depth was reduced to 75 mm and only one injection case was investigated. The injection point was at the main channel/flood plain interface, $y = 100$ mm. For the numerical model simulation, the Schmidt number

$$\sigma_k = \frac{\nu_r}{D} = 1.0 \quad (14)$$

was again used. The measured and computed concentration distributions are shown in Figure 9. The experimentally measured concentration profile has two concentration peaks occurring at $y = 90$ mm with a magnitude of 4.0 ppb and at $y = 135$ mm with a magnitude of 5.0 ppb, the dye having spread over 70% of the channel width. Both models predict concentration distributions with one peak and its magnitudes higher than that was measured, and the spreading of the dye across the channel is less. This implies that the models under-predict lateral mixing.

10 Discussion of results

The numerical predictions of transverse distribution of concentration at $z = 105$ mm, shown in Figure 5, are all lower and narrower than the experimental data, indicating under-prediction of mixing. This is because of the spreading of the dye vertically and laterally in the channel. The more the dye spread, the higher the eddy diffusivity. The under prediction of the mixing is therefore due to either the predicted eddy viscosity being too low, or the turbulent Schmidt number being too high. The

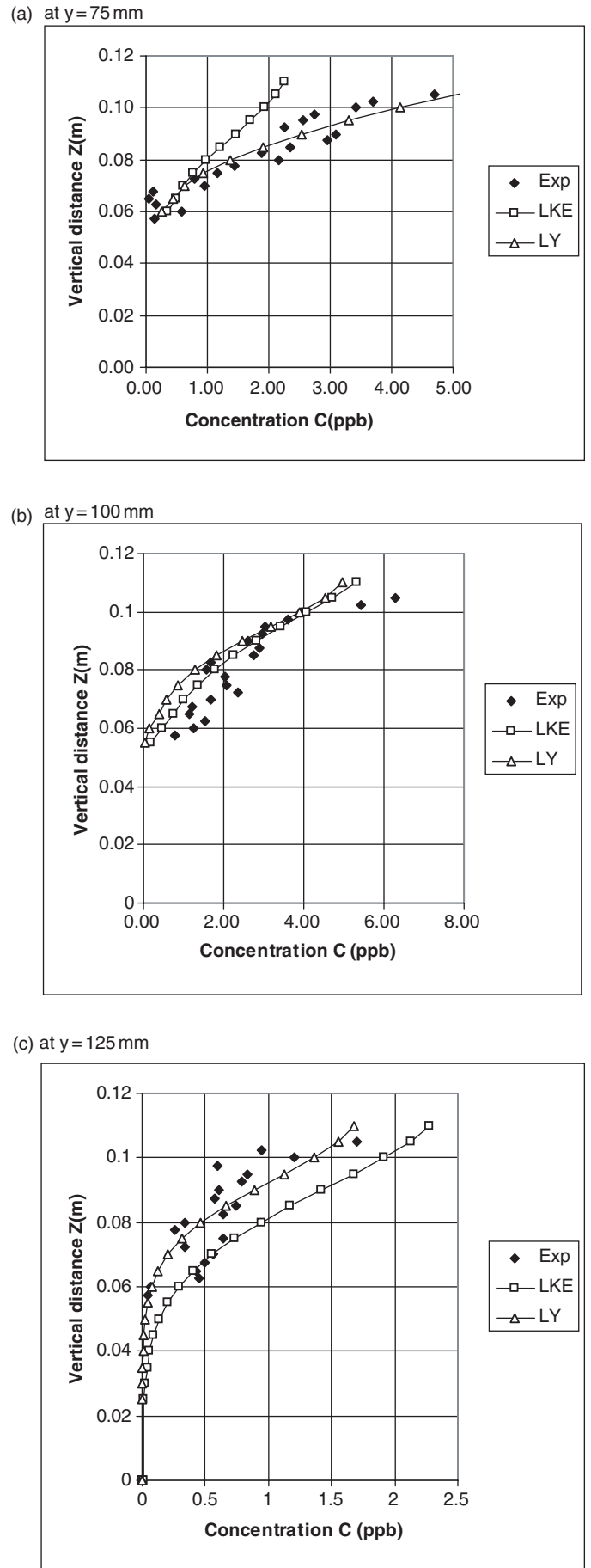
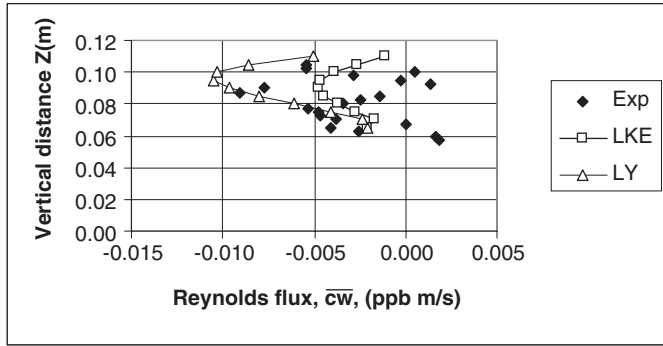
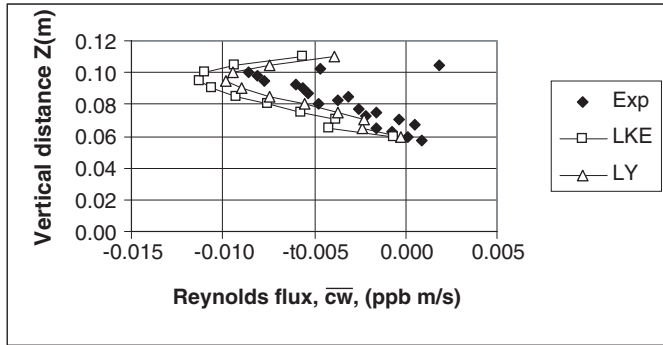


Figure 7 Mean concentration distributions of experimental data and model results for 100 mm injection.

(a) at $y = 75$ mm



(b) $y = 100$ mm



(c) at $y = 125$ mm

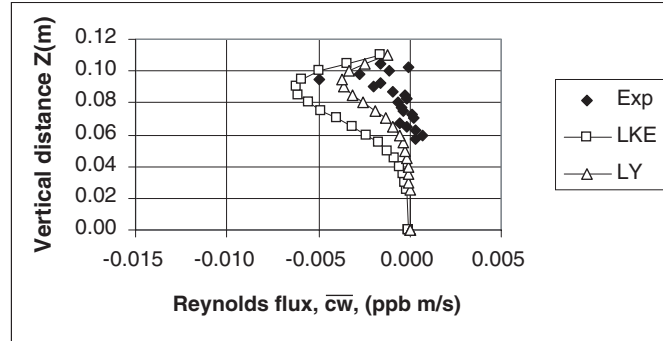


Figure 8 Reynolds flux, $\bar{c}w$, distributions of experimental data and model results for 100 mm injection point.

non-dimensional eddy diffusivities at $z = 105$ mm predicted by the LKE and LY models with $\sigma_k = 1.0$ and together with the experimental data near peak Reynolds flux areas for the three injection cases are shown in Figure 10. The LKE model predicts 18% higher averaged non-dimensional eddy diffusivity ($=0.47$) across the channel width than that ($=0.385$) of the LY model, similarly about 20% higher the depth averaged non-dimensional eddy viscosity of LKE calculated than that of LY. The predicted eddy diffusivities are smaller than the measured averaged value of 0.0728 although the measured data are scattered. The averaged value of the non-dimensional eddy viscosity from the measured data as shown in Figure 10 is 0.0701 and close to the measured non-dimensional eddy diffusivity value. The calculated eddy viscosity by LY model is therefore under-valued. The ratio of the predicted averaged eddy viscosity to the measured averaged eddy diffusivity is 0.55. This value is within the range found in previous studies, such as Arnold *et al.* (1985) who experimentally measured σ_k between 0.4 and 1.0. The most recent numerical

At $y = 100$ mm injection

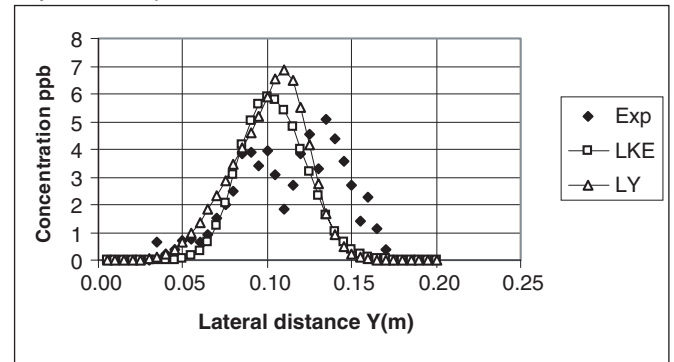


Figure 9 Mean concentration distributions of experimental data and model results at $z = 70$ mm for shallow flood water depth ($Dr = 0.27$).

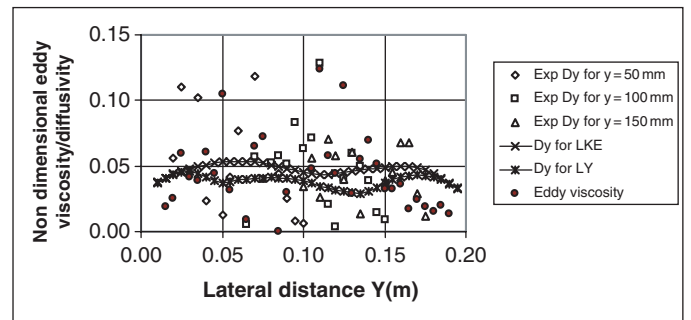


Figure 10 Lateral eddy diffusivity/viscosity distributions of experimental data and model results near water surface.

model study using a LKE model (Simoes and Wang, 1997) used $\sigma_{ky} = 0.5$, which nearly agrees with our estimated $\sigma_{ky} = 0.55$. However the ratio of the measured eddy viscosity to the measured eddy diffusivity is 0.963 or nearly 1.0.

There is lower peak concentration in the main channel than those on the floodplain as shown in Figure 5. The variation in peak concentration is due to variation of the eddy viscosity. The predicted eddy viscosity across the channel showed larger eddy viscosity in the main channel larger than on the flood plain. Previous experiments by Wood and Liang (1989) concluded that releasing an effluent in the main channel as opposed to the flood plain produces a higher degree of mixing. This is confirmed in the present experiments and by the model predictions, the cause being identified as the higher eddy viscosity in the main channel as compared to the flood plain.

In C2 and C3, the prediction of mixing is generally good, with concentration gradients being predicted well, as already shown in Figure 5. The gradient $\partial C / \partial y$ of concentration is an indication of turbulent mixing if there is no secondary flow, but there is an additional effect of the advection by secondary flow on the distribution of concentration. The effect of secondary flow is more noticeable in C2, than was in C1 and C3. The position of the concentration peak predicted by the LY model is significantly shifted laterally away from the injection point (see Figure 5). There are a mild gradient on the left side of the concentration peak and a steep gradient on the right side. According to at Figure 10, the eddy viscosity is decreasing from the main channel to the floodplain where the concentration gradient is mild, and also the eddy viscosity decreases and increases in the steep gradient region. It

does not follow that the smaller the eddy viscosity the steeper the gradient. This is an example of how the secondary flow can indirectly affect the mixing by differential transport rates across the channel. In the Main/Floodplain region, the dye is being carried on either sides of the Main/Floodplain interface by the twin vortices and being stretched either sides of the M/F interface, hence mild gradient of the dye concentration. However the dye is being carried onto the flood plain, but there is the opposite direction of secondary flow to one of the twin vortices which prevents transporting the dye outwards the floodplain wall. This mechanism in the meeting place of the secondary flow cells stops transporting the dye and hence steepening the concentration gradient.

The vertical concentration profiles give a good indication of whether the mixing is being over-predicted over the water depth. As shown in Figure 11, the concentration profiles illustrate how over and under prediction of mixing can be identified. From this we can infer that, in Figure 7, at $y = 75, 100$ and 125 mm, the mixing is over predicted by both models because the predicted gradient of concentration is milder in the upper layer and steeper in the lower layer than those of the experimental data. At $y = 75$ and 100 mm, the flux is also over-predicted possibly indicating that σ_k controlling vertical mixing is too low. This agrees that both models over predict the eddy diffusivity in the shear layer region as shown in Figure 12. Therefore the vertical eddy diffusivity needs to be reduced for better predictions in this study, meaning the turbulent Schmidt number needs to increase. The above discussion suggests that the turbulent diffusion coefficient is an an-isotropic. This agrees with the study by Simoes and Wang (1997) who obtained the best results with an an-isotropic eddy diffusivity that used $\sigma_{ky} = 0.5$ and $\sigma_{kz} = 1.0$. Numerous studies on the lateral diffusion coefficient show that σ_{ky} is in the range between 0.5 and 1.0, but σ_{kz} is generally unity. However, the above comparative study on the vertical distribution of the dye concentration and the diffusion coefficient suggests the need to change of σ_k in order to compensate an inaccurate prediction of eddy viscosity. From the result of optimisation of the turbulent

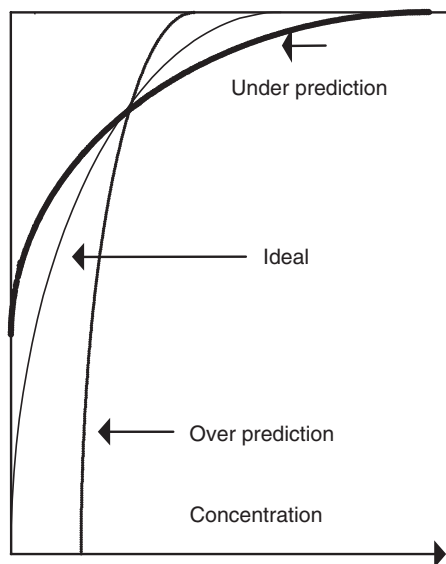


Figure 11 Typical concentration vertical profiles.

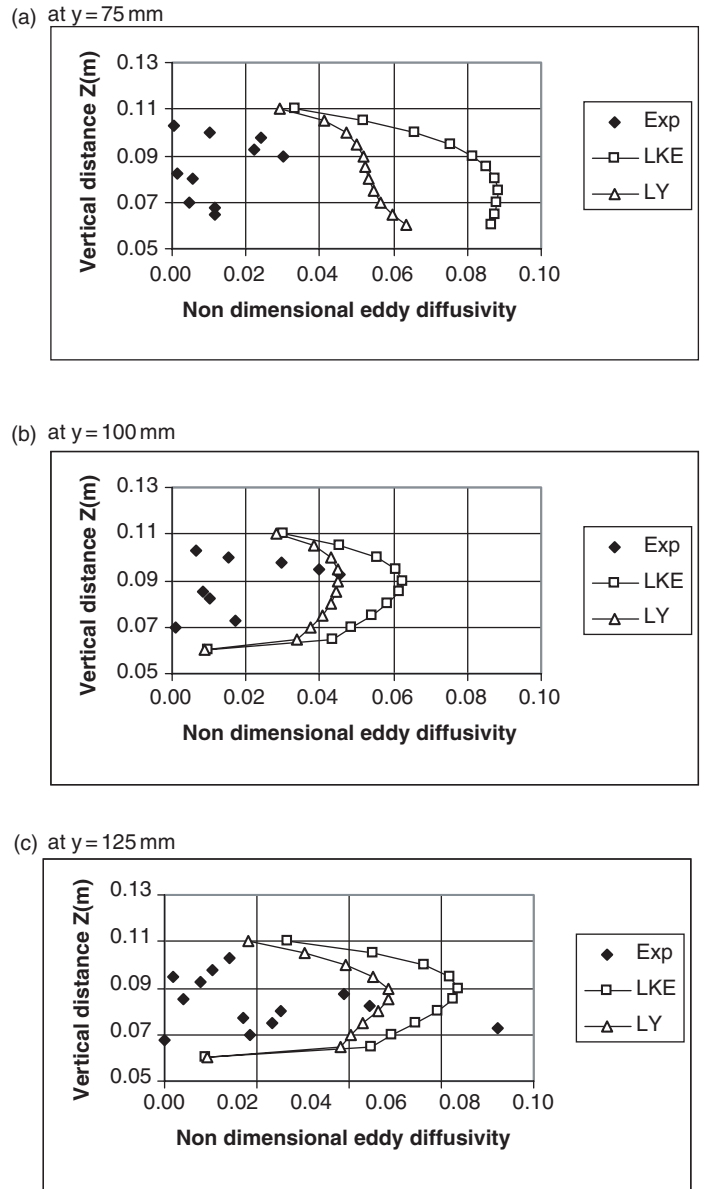


Figure 12 Eddy diffusivity distributions of experimental data and model results for 100 mm injection point.

Schmidt numbers, $\sigma_{ky} = 0.75$ and $\sigma_{kz} = 1.5$ gave the best result as shown in Figure 13. It follows that even if a model does not predict eddy viscosity correctly, solute concentration can be reasonably well predicted by adjusting the turbulent Schmidt number as demonstrated here. However the hydrodynamic model needs to be improved for more accurate prediction of eddy viscosity, since otherwise the turbulent Schmidt number is required to change.

For the shallow flood water case, the experimentally measured concentration profile has two concentration peaks, but both numerical models do not predict these two peaks, instead showing the one peak concentration as found with the deeper compound channel. A possibility of this is when flooding occurs in a shallow flooded water case, large difference in velocities between the main channel and the floodplain generates large horizontal eddies (organised planform vortices) in the shear layer, observed first by Sellin (1964) and later Fukuoka and Fujita (1989) and Ikeda *et al.* (1995), based on laboratory studies. Both models used here were not able to predict large horizontal eddies. For shallow flooded

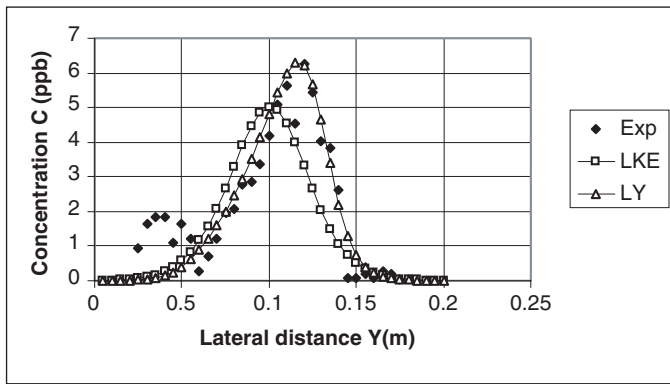


Figure 13 Concentration distributions for Turbulent Schmidt numbers of 0.75 and 1.5.

water the organized planform vortices is predominant for mixing and transporting dye but not for deep flooded water. For deep flooded water, secondary flow is predominant (see Nezu, 1996). Hence the prediction of dye concentration distributions for the deep flooded water is reasonably good. Large Eddy Simulation (LES), (Thomas and Williams, 1995) produces large horizontal eddies in a compound channel, therefore it remains to be seen whether LES can predict two peaks.

In order to investigate the effects of secondary flow on peak concentration in the shear layer along the channel for deep flooded water, using both LKE and LY models, dye was released at $y = 0.1$ m near the water surface. The turbulent Schmidt numbers were set to one for both models. Lateral distributions of dye concentration along the channel were predicted and are shown in Figure 14. The longitudinal distance was normalized using the main channel water depth. It can be clearly seen from the figure that there are two main features. One the magnitudes of peak concentration between the LKE and LY results are different. The other the location of concentration peak stays almost in line of the dye injection point for the LKE model result, but drifts for the LY model result. As shown in Figure 14c, both peak concentrations decrease exponentially along the channel and the ratio of the peak concentration of the LKE model result to that of the LY model result, in terms of %, is about 20% or more along the channel. The difference in the magnitudes is reflected by the difference in eddy viscosities in both models. Figure 14d shows an interesting result that indicates the effect of secondary flow on concentration peak along the channel. The drifting distance of concentration peak in line with the injection point, normalized by the main channel water depth, increases linearly to $x/H = 18$ and stays the same line after this point. Near the injection field, the transporting concentration peak seems to be purely with the longitudinal velocity and secondary currents. For example, the average values $U = 0.3$ m/s and $V = 0.004$ m/s found in this study give an angle of peak moving in line with the injection point and a peak drifting a distance of 27 mm when $x = 2$ m ($x/H = 18$) which is half a secondary flow cell size. The size of secondary flow cell on the flood-plain is roughly the floodplain water depth (~ 50 mm) (see Figure 4b). After a certain distance, there is little drift in the peak. This indirectly demonstrates that the width of stream-lines on the water surface normally observed in a river is well known as a size of secondary flow cell.

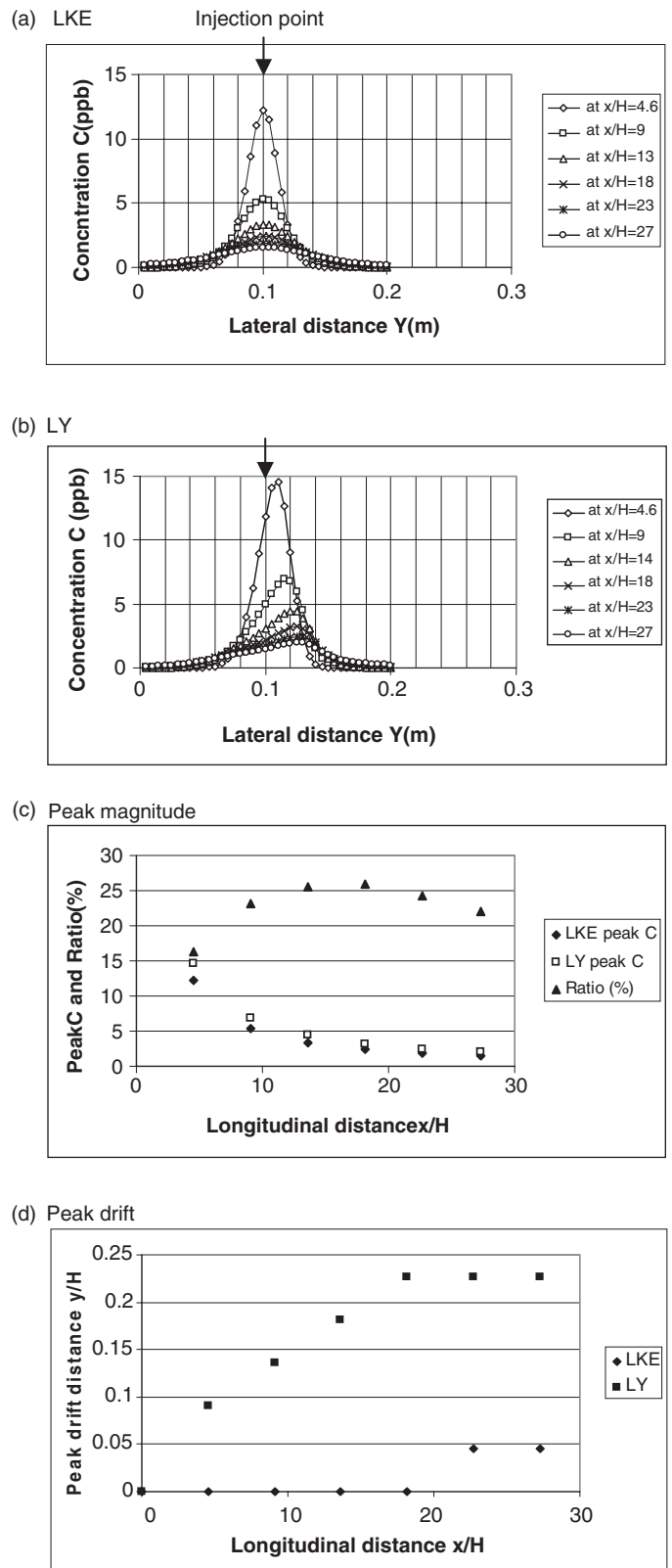


Figure 14 Longitudinal variations of concentration peak.

11 Conclusions

- (1) Predictions of local velocity in the shear layer using the LY model were in good agreement with the experimental data, but not so good using the LKE model because the model was unable to predict secondary flow. Generation of

secondary flow by a numerical model is an important factor to accurately predict local velocity. The LY model reasonably accurately predicted secondary flow in the shear layer, but the inclination angles of two vortices from the edge of the main/floodplain junction were slightly steeper than that was measured.

- (2) For deep flooded water, the LKE and LY models predicted lateral distributions of dye concentration near the water surface for 3 dye injection points. Predicted concentration peaks on the flood plain are higher than that in the main channel, which is reflected by the magnitude of eddy viscosity. This is also consistent with the experimental results obtained by Wood and Liang (1989). The LKE model predicted a distribution similar to a Gaussian distribution in all injection cases, but the LY model predicted a skewed distribution in the shear layer in particular, which agrees the experimental data very well. The cause of the skewed distribution was found to be due to secondary flow.
- (3) The LY and LKE models predicted vertical distributions of dye concentration in the shear layer and compared it with the experimental data. As a result of comparisons the mixing is over predicted by both models.
- (4) From the comparison between the measured and computed eddy diffusivities, the turbulent Schmidt numbers are not unity in both vertical and lateral directions, which agrees with the previous work by Simoes and Wang (1997). In this study, from the results of optimisation, turbulent Schmidt numbers of $\sigma_{ky} = 0.75$ and $\sigma_{kz} = 1.5$ gave the best result. If a model predicts eddy viscosity incorrectly, the change of the turbulent Schmidt number will give a better prediction of solute concentration. However the hydrodynamic model needs to be improved for a more accurate prediction of eddy viscosity.
- (5) For shallow flooded water the experimental lateral distribution of dye concentration has two concentration peaks, but both models have not successfully predicted it. Large horizontal eddies occurring in the shallow flooded water might be responsible for producing the two peaks. Both models used were not able to predict this phenomenon, but Large Eddy Simulation (LES) is known to produce large horizontal eddies in a compound channel. Therefore it remains to be seen whether LES can predict two peaks.
- (6) The effect of secondary flow on peak concentration in the shear layer along the channel for deep flooded water was observed to be very significant near the injection point. The position of the peak was linearly shifted with the ratio of the longitudinal velocity to the lateral velocity until its distance became half a secondary flow cell size on the floodplain. The peak concentration was more than 20% different in the models with and without a secondary flow modelling capability.

References

1. ARNOLD, U., PASCHE, E. and ROUVE, G. (1985). "Mixing in Rivers of Compound Cross Section", *Proc. 21st IAHR Congress*, Melbourne, Australia, August 1985, pp. 168–172.
2. COKLIAT, D. and YOUNIS, B. (1995). "Second Order Closure Study of Open-channel Flows", *J. Hydr. Engrg.* ASCE, 121, 94–107.
3. DJORDJEVIC, S. (1993). "Mathematical Model of Unsteady Transport and its Experimental Validation in Compound Open Channel Flow", *J. Hydr. Res.*, 31(2), 229–248.
4. FUKUOKA, S. and FUJITA, K. (1989). "Prediction of Flow Resistance in Compound Channels and its Application to Design of River Courses", *Proc. JSCE*, 411, 63–72, (in Japanese).
5. IKEDA, S., MURAYAM, N. and KUGA, T. (1995). "Stability of Horizontal Vortices in Compound Open Channel Flow and their 3-D Structure", *J. Hydr., Coastal and Environ. Engrg.* JSCE, 509/II-30, 131–142, (in Japanese).
6. KAWAHARA, Y. and TAMAI, N. (1988). "Numerical Calculation of Turbulent Flows in Compound Channels with an Algebraic Stress Turbulence Model", *Proc. 3rd Int. Symp. on Refined Flow Modelling and Turbulence Measurements*, Tokyo, 9–17.
7. KEARNEY, D.J. (2000). "Turbulent Diffusion in Channels of Complex Geometry", Ph.D thesis, Loughbough University.
8. LAUDER, B.E. and YING, W.H. (1973). "Prediction of Flow and Heat Transfer in Ducts of Square Cross Section", *Proc. Instn. Mech. Engrs.*, 187, 455–461.
9. LIN, B. and SHIONO, K. (1995). "Numerical Modelling of Solute Transport in Compound Channel Flows", *J. Hydr. Res.*, 33(6), 1995, 773–788.
10. NAOI, D. and RODI, W. (1982). "Calculation of Secondary Currents in Channel Flow", *J. Hydr. Div., Proc. American Society of Civil Engineers*, 108, 948–968.
11. NAOI, D., NEZU, I. and NAKAGAWA, H. (1993). "Hydrodynamic Behaviour of Compound Rectangular Open Channels", *J. Hydr. Engrg.*, 119(3), 390–408.
12. NEZU, I. (1996). "Experimental and Numerical Study on 3-D Turbulent Structures in Compound Open-channel Flows", *Flow Modeling and Turbulence Measurements* (ed. C.J. Chen), Balkema, pp. 65–74.
13. NOKES, R.I. and HUGHES, G.O. (1994). "Turbulent Mixing in Uniform Channels of Irregular Cross-section", *J. Hydr. Res.*, 32, 67–86.
14. NOKES, R.I. and WOOD, I.R. (1988). "Vertical and Lateral Turbulent Dispersion: Some Experimental Results", *J. Fluid Mech.*, 187, 373–394.
15. PATANKER, S.V. and SPALDING, D.B. (1972). "A Calculation Procedure for Heat, Mass and Momentum Transfer in Three Dimensional Parabolic Flows", *Int. J. Heat Mass Transfer*, 15, 1787–1806.
16. PEZZINGA, G. (1994). "Velocity Distribution in Compound Channel Flows by Numerical Modelling", *J. Hydr. Engrg.*, 120(10), 1176–1198.
17. PRINOS, P. (1992). "Dispersion in Compound Open Channel Flow", *Hydraulic and Environmental Modelling: Estuarine*

- and River Waters, Ed. Falconer, Shiono, Matthew, Ashgate publishing Ltd., pp. 359–372.
18. RODI, W. (1980). Turbulence Models and their Application in Hydraulics, a State of the Art Review, IAHR, Delft.
 19. SELLIN, R.H.J. (1964). “A Laboratory Investigation in to the Interaction between Flow in the Channel of a River and that of its Floodplain”, *La Houille Blanche*, 7, 793–801.
 20. SHIONO, K. and FENG, T. (2003). “Turbulence Measurements of Dye Concentration and the Effect of Secondary Flow on its Distribution in Open Channel Flows”, *J. Hydraul. Engrg.* ASCE, in press.
 21. SHIONO, K. and KNIGHT, D. (1991). “Turbulent Open Channel Flows with Variable Depth Across the Channel”, *J. Fluid Mech.*, 222, 617–647.
 22. SHIONO, K. and LIN, B. (1992). “Three Dimensional Numerical Models for Two Stage Open Channel Flows”, *Hydrocomp '92, Inter. Conference of Computational Methods and Measurements in Hydraulics and Hydrology*, Ed. Gayer, Starosolszky, Maksimovic, pp. 123–130.
 23. SIMOES, F.J.M. and WANG, S.S.Y. (1997). “Numerical Prediction of Three Dimensional Mixing in a Compound Channel”, *J. Hydr. Res.* IAHR, 5, 619–642.
 24. SPEZIALE, C. (1987). “On Linear $k-l$ and $k-\varepsilon$ Models of Turbulence”, *J. Fluid Mech.*, 178, 459–475.
 25. THOMAS, T. G. and WILLIAMS, J.J.R. (1995). “Large Eddy Simulation of a Symmetric Trapezoidal Channel at a Reynolds Number of 430,000”, *J. Hydr. Res.*, 33, 27–41.
 26. TOMINAGA, A. and NEZU, I. (1991). “Turbulent Structure in Compound Open Channel Flows”, *J. Hydr. Engrg.*, 117(1), 21–41.
 27. WOOD, I.R. and LIANG, T. (1989). “Dispersion in an Open Channel with a Step in the Cross-section”, *J. Hydr. Res.*, 27(5), 1989, 587–601.